Orientation of linear molecules in two-color laser fields with perpendicularly crossed polarizations

Je Hoi Mun,[1,*] Hirofumi Sakai,[2,3,†] and Rosario González-Férez[4,‡]

[1]*Center for Relativistic Laser Science, Institute for Basic Science (IBS), Gwangju 61005, Republic of Korea*

[2]*Department of Physics, Graduate School of Science, The University of Tokyo, 7-3-1 Hongo, Bunkyo-ku, Tokyo 113-0033, Japan*

[3]*Institute for Photon Science and Technology, Graduate School of Science, The University of Tokyo, 7-3-1 Hongo, Bunkyo-ku, Tokyo 113-0033, Japan*

[4]*Instituto Carlos I de Física Teórica y Computacional, and Departamento de Física Atómica, Molecular y Nuclear, Universidad de Granada, 18071 Granada, Spain*

(Received 19 February 2019; published 30 May 2019)

Molecular orientation methods based on nonresonant two-color laser pulses having parallel polarizations have been reported theoretically and experimentally. In this work, we demonstrate that perpendicularly polarized two-color laser fields can be used to achieve stronger molecular orientation when nanosecond laser pulses are used. The two-color fields align the molecules to the two-dimensional plane parallel to the field polarization; at the same time, they orient the molecules in the direction of the 2ω polarization. We show that the interplay between the interactions due to the ω- and 2ω-laser fields provides stronger molecular orientation than the parallel field configuration. This is due to temporally synchronized generations of alignment and orientation, which reduce the nonadiabatic effects.

DOI: 10.1103/PhysRevA.99.053424

I. INTRODUCTION

Control of the directional features of molecules, by inducing their alignment and/or orientation, is an important tool for experimental studies performed in the laboratory-fixed frame. The alignment techniques are well established and have been utilized in many interesting applications, such as multiphoton ionization [1], photoelectron angular distributions [2], and molecular imaging based on high-order harmonic generation [3–6].

Molecules are aligned when the molecule-fixed axes are confined along the laboratory-fixed frame. Alignment is based on the interaction of the molecular anisotropic polarizability and a nonresonant moderately strong laser field [7,8]. Due to the plus-minus inversion symmetry of the laser field, molecules are aligned along the polarization of the field without the head-versus-tail order confinement. By breaking this inversion symmetry, the molecular electric dipole moment can be confined to a particular direction, and polar molecules become oriented. Among various experimental techniques, combined electrostatic and nonresonant laser fields (combined fields) [9–13], a phase-locked two-color laser field [14,15], and THz pulses [16–18] create samples of oriented molecules.

For a molecular beam formed from different rotational states, e.g., a thermal ensemble, the degree of alignment is increased by simply increasing the intensity of the nonresonant laser pulse. In contrast, the rotational states might be oriented in opposite directions, and, as a consequence, the orientation of a molecular beam might be moderate or even small. Particular experimental efforts have been undertaken to improve the orientation of molecular samples. A solution to overcome this difficulty is the orientation of state-selected molecular beams created by an electrostatic deflector [13,19–21] or a hexapole focuser [22]. Another solution is using one-color and delayed two-color femtosecond laser pulses, which selectively orients half of the rotational states in the same direction [23–27].

In spite of these experimental advances, nonadiabatic processes prevent one from reaching a high degree of orientation even when nanosecond laser pulses are used. The nonadiabatic rotational dynamics provokes transitions between oppositely oriented adiabatic pendular states contributing to the field-dressed wave function [28]. As a consequence, the orientation is significantly reduced in comparison to the predictions of the adiabatic approximation [28,29], whereas the alignment is not affected because these two states lead to the inversion-symmetric alignment [30]. For the combined-field orientation technique, the angle between the fields, the laser pulse width, and the strength of the electrostatic field, as well as the initial state play crucial roles in the field-dressed rotational dynamics, and become control knobs to reach higher degrees of orientation [28–33]. For the two-color laser field technique, the orientation obtained by solving the time-dependent Schrödinger equation does not agree with the results from the adiabatic approximation [34]. Possible solutions to reach an adiabatic orientation were investigated for two-color laser fields with parallel polarizations [34]. Thus, to reach an adiabatic control of the field-dressed dynamics has become a challenging subject to achieve higher degrees of molecular orientation.

In this work, we propose the orientation of linear molecules using nonresonant two-color laser fields with perpendicularly crossed polarizations. Analogous to the parallel-polarized two-color field case, due to the interaction with the molecular

*mun1219@ibs.re.kr
†hsakai@phys.s.u-tokyo.ac.jp
‡rogonzal@ugr.es

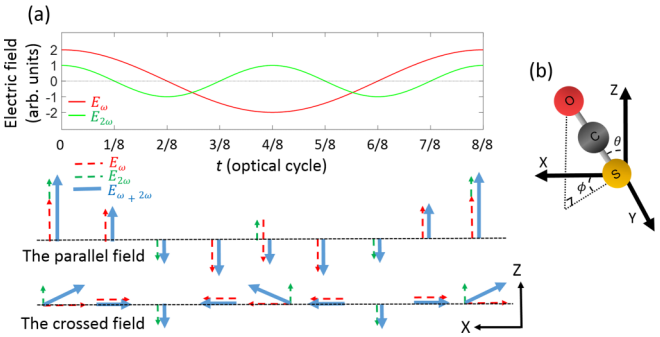

FIG. 1. (a) Temporal evolutions of the electric-field components of parallel and perpendicularly polarized two-color laser fields during one optical cycle of the ω-laser pulse. (b) A sketch (not to scale) of a triatomic linear molecule OCS and the Euler angles (θ, ϕ). The degree of orientation along the Z axis, and the degrees of alignment along the Z and X axes are given by $\langle\cos\theta\rangle$, $\langle\cos^2\theta\rangle$, and $\langle\sin^2\theta\,\cos^2\phi\rangle$, respectively.

hyperpolarizability, pendular states with different parity are coupled. Thus asymmetry with respect to the plus-minus inversion of the polarization direction of the 2ω-laser field is introduced and the molecules are oriented. Such a crossed-polarization configuration was theoretically investigated for three-dimensional orientation of chiral molecules in the adiabatic regime [35]. We propose that the crossed-polarization configuration can be used for achieving stronger orientation of linear molecules. We provide an explicit orientation Hamiltonian of a linear molecule interacting with two-color laser fields with perpendicularly crossed polarizations. The field-dressed rotational dynamics is analyzed by solving the time-dependent Schrödinger equation (TDSE) and by the adiabatic approximation (AA).

In an experimental configuration with nanosecond two-color laser pulses, the second harmonic pulse has a shorter temporal width than the fundamental pulse. Hence, for parallel fields, the alignment is created by the ω-laser field having a longer temporal width. Once the interaction with the 2ω-laser field becomes significant, the molecules are also oriented due to the coupling of the pendular states having opposite parity. In this delayed creation of the orientation, a significant discrepancy between the TDSE and the AA was pointed out [34]. For perpendicular fields, the X-polarized ω-laser field aligns first the molecules in the X direction (see Fig. 1). When the intensity of the 2ω-laser field polarized along the Z direction increases and exceeds that of the ω-laser field, the molecules become aligned and oriented toward the Z direction. In this way, the alignment and orientation potentials along the Z axis are generated simultaneously. We show here that this gives rise to better adiabaticity and to stronger molecular orientation.

The paper is organized as follows. In Sec. II, we derive the Hamiltonian describing the interaction of a molecule and two-color laser fields with parallel and perpendicular polarizations. The symmetries of the Hamiltonian and the numerical methods are also explained in Sec. II. The field-dressed rotational dynamics for parallel and perpendicular fields is discussed in Sec. III. A summary and an outlook are provided in Sec. IV.

II. HAMILTONIAN OF THE SYSTEM

We assume the Born-Oppenheimer and rigid rotor approximations to describe the rotational dynamics of linear polar molecules. Within this framework, the Hamiltonian of a field-free linear polar molecule reads

$$H_{\rm rot} = B\vec{J}^{\,2}, \tag{1}$$

where B and $\vec{J}$ are the rotational constant and the angular momentum operator, respectively.

When the external electric field is moderately strong (10^{10}–10^{12} W/cm^2), the light-molecule interaction Hamiltonian is given by the low-order perturbation theory [36]

$$H_{\rm int} = -\sum_i \mu_i E_i - \frac{1}{2!}\sum_{ij}\alpha_{ij}E_iE_j - \frac{1}{3!}\sum_{ijk}\beta_{ijk}E_iE_jE_k - \cdots, \tag{2}$$

where μ is the permanent dipole moment vector, α the polarizability tensor, and β the hyperpolarizability tensor. In this expression (2), the electric field components, E_i with $i = x, y, z$, are expressed in the molecule-fixed frame, and we need to relate them with the laboratory-fixed frame components. The transformation between both reference frames is given in Appendix A.

We consider two-color laser fields, with the two electric-field components having either parallel polarizations

$$\vec{E}^{\,\parallel}(t) = E_\omega(t)\cos(\omega t)\vec{e}_Z + E_{2\omega}(t)\cos(2\omega t)\vec{e}_Z \tag{3}$$

or perpendicular polarizations

$$\vec{E}^{\,\perp}(t) = E_\omega(t)\cos(\omega t)\vec{e}_X + E_{2\omega}(t)\cos(2\omega t)\vec{e}_Z, \tag{4}$$

where $E_\omega(t) \equiv E_{\omega,0}\exp(-t^2/2\tau_\omega{}^2)$ and $E_{2\omega}(t) \equiv E_{2\omega,0}\exp(-t^2/2\tau_{2\omega}{}^2)$ are the envelopes of the ω- and 2ω-laser fields, respectively. $E_{\omega,0}$ ($E_{2\omega,0}$) is the peak strength of the ω-laser (2ω-laser) field and $\tau_{\omega(2\omega)}$ is related to the FWHM $= 2\tau_{\omega(2\omega)}\sqrt{2\ln 2}$. The phase difference between the two electric fields is fixed at zero throughout the paper. The evolutions of the electric field components are plotted in Fig. 1(a).

Since we further assume that the frequencies of the ω- and 2ω-laser fields are far from any molecular resonance and much higher than the rotational frequency of the molecule, we can average over the rapid oscillations of the nonresonant laser fields. Then, the linear term in Eq. (2), which involves the electric dipole moment, vanishes, whereas the second and third terms provide the alignment and orientation interactions, which for parallel fields take the following expressions [14]:

$$H^{\parallel}_{\rm int}(t) = H^{\parallel}_{\rm align}(t) + H^{\parallel}_{\rm orient}(t), \tag{5}$$

$$H^{\parallel}_{\rm align}(t) = -\frac{1}{4}[E_\omega(t)^2 + E_{2\omega}(t)^2]\Delta\alpha\,\cos^2\theta, \tag{6}$$

$$H^{\parallel}_{\rm orient}(t) = -\frac{1}{8}E_\omega(t)^2E_{2\omega}(t)[3\beta_{zxx}\cos\theta + (\beta_{zzz} - 3\beta_{zxx})\cos^3\theta], \tag{7}$$

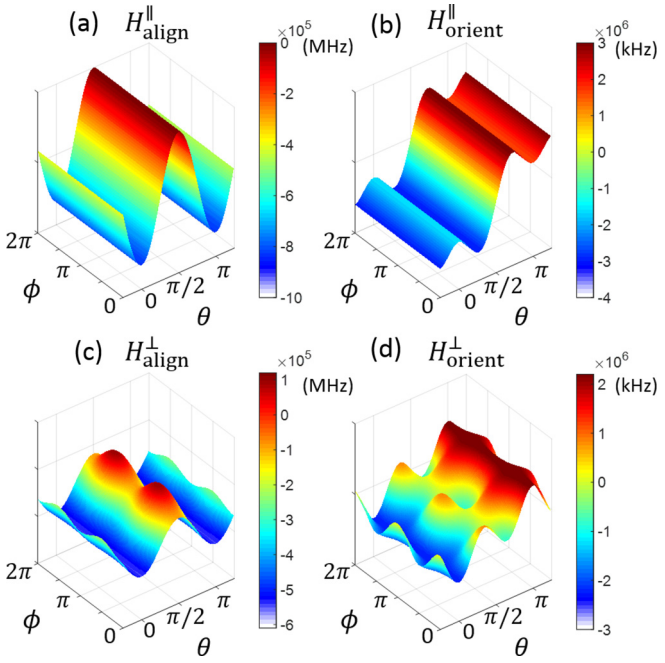

FIG. 2. For parallel fields, (a) and (b) show alignment and orientation Hamiltonians (6) and (7), respectively, as a function of the Euler angles in units of π. For perpendicular fields, (c) and (d) show alignment and orientation Hamiltonians (9) and (10), respectively, as a function of the Euler angles in units of π. The peak intensities are $I_{\omega,0} = 3.0 \times 10^{11}$ W/cm^2 and $I_{2\omega,0} = 10^{12}$ W/cm^2. The interaction potentials are expressed in units of Hz.

where $\Delta\alpha = \alpha_{zz} - \alpha_{xx}$ is the polarizability anisotropy with α_{zz} and α_{xx} being the polarizability components parallel and perpendicular to the molecular axis; β_{zzz} and β_{zxx} are the hyperpolarizability components parallel and perpendicular to the molecular axis. In Eqs. (6) and (7), we have omitted the terms independent of θ and ϕ because they only represent an energy shift. The molecular alignment along the Z axis is due to the double-well potential of Eq. (6), with two minima localized at $\theta = 0$ and $\theta = \pi$ as shown in Fig. 2(a). The strength of this alignment interaction is determined by the total intensity of the nonresonant laser fields. The orientation term (7) shows an asymmetry in θ and the deepest well is located near $\theta = 0$ [see Fig. 2(b)]. As a consequence, the molecules tend to be oriented along the $+Z$ direction. The maximal strength of the orientation term (7) is smaller than the maximal alignment strength given by the Hamiltonian (6), by approximately two orders of magnitude.

Analogously, for the perpendicular-field configuration, the interaction Hamiltonians read

$$H^{\perp}_{\rm int}(t) = H^{\perp}_{\rm align}(t) + H^{\perp}_{\rm orient}(t), \tag{8}$$

$$H^{\perp}_{\rm align}(t) = -\frac{1}{4}\Delta\alpha\left[\left(E_{2\omega}(t)^2 - \frac{E_{\omega}(t)^2}{2}\right)\cos^2\theta + \frac{1}{2}E_{\omega}(t)^2\sin^2\theta\,\cos 2\phi\right], \tag{9}$$

$$H^{\perp}_{\rm orient}(t) = -\frac{1}{16}E_{\omega}(t)^2E_{2\omega}(t)[(\beta_{zzz} - \beta_{zxx})\cos\theta - (\beta_{zzz} - 3\beta_{zxx})(\cos^3\theta - \sin^2\theta\,\cos 2\phi\,\cos\theta)]. \tag{10}$$

The ω- and 2ω-laser field components of $H^{\perp}_{\rm align}(t)$ are confined to the XZ plane, and force the molecules to align along the X and Z axes, respectively. The molecules are actually aligned along a polarization direction of the stronger laser field between the ω- and 2ω-laser pulses. At the same time, the two-color perpendicular fields also generate an orientation potential asymmetric upon the plus-minus inversion of the Z direction. As we demonstrate in Sec. III, the orientation in the Z direction can be significant only when the alignment along the same Z direction also exists. These potentials (9) and (10) are plotted in Figs. 2(c) and 2(d), respectively. Compared to the parallel-field configuration, these alignment and orientation potentials show a more complicated dependence on the Euler angles (θ, ϕ). Again, the interaction with the molecular polarizability is the dominant one.

When the two electric fields have parallel polarizations, the total Hamiltonian $H = H_{\rm rot} + H^{\parallel}_{\rm int}(t)$ is invariant under the rotations around the Z axis. This symmetry ensures that the magnetic quantum number M is preserved. In this case, the TDSE is solved by expanding the wave function in terms of the spherical harmonics with fixed M. For two-color laser fields with perpendicular polarizations, the total Hamiltonian $H = H_{\rm rot} + H^{\perp}_{\rm int}(t)$ couples field-free states with different magnetic quantum numbers, but is invariant under the reflection about the XZ plane. We then solve the TDSE using a basis set expansion of the wave function in terms of functions that reflect this symmetry. In particular, we employ the Wang basis set [29,32] constructed from linear combinations of the spherical harmonics with the proper parity under the reflection about the XZ plane. For $M > 0$, these states are defined as

$$|J, M, s\rangle \equiv \frac{1}{\sqrt{2}}[|J, M\rangle + (-1)^s|J, -M\rangle], \tag{11}$$

where $s = 0$ or 1, and for $M = 0$,

$$|J, M, s = 0\rangle \equiv |J, 0\rangle. \tag{12}$$

In these basis functions, the parity of $M + s$ is the preserved quantity. This can be checked by multiplying the σ_{ZX} operator, which gives the reflection in the XZ plane, to the Wang basis set. σ_{ZX} changes the plus-minus sign of ϕ [29], which means that the spherical harmonic $|J, M\rangle$ converts to $(-1)^M|J, -M\rangle$. The wave functions constructed by the Wang basis set have either even or odd parity depending on $M + s$.

Thus the TDSE is solved independently in the two irreducible representations of this symmetry. The nonzero matrix elements of the Hamiltonian matrices are summarized in Appendix B.

To solve the TDSE, we employ the time-dependent unitary transformation method. For every time step, we calculate the eigenstates and the corresponding eigenenergies of the field-dressed time-independent Hamiltonian. In a single time step, an initial wave function is expanded by the eigenstates of the field-dressed Hamiltonian. The time evolution of the

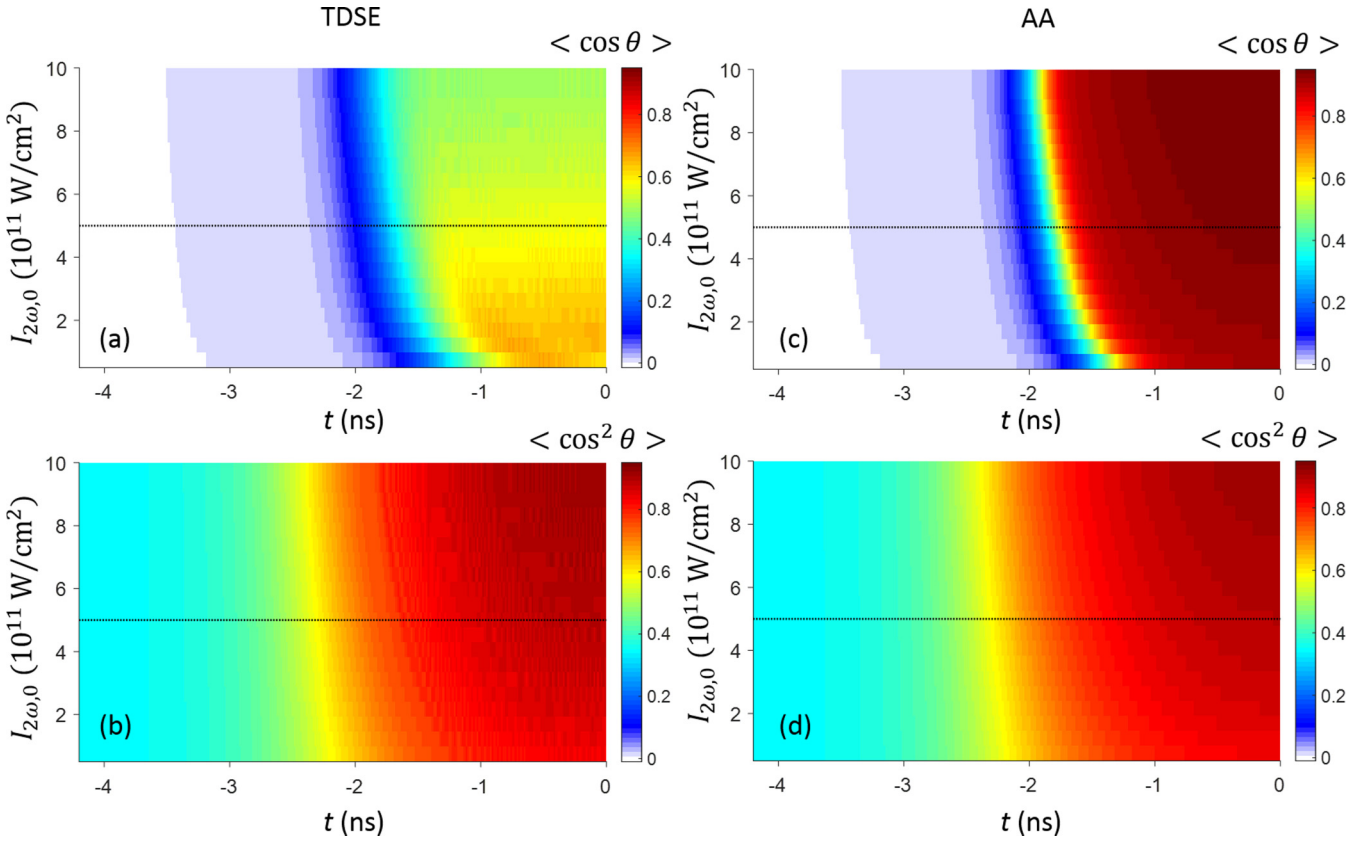

FIG. 3. For parallel fields, (a) orientation $\langle \cos\theta \rangle$ and (b) alignment $\langle \cos^2\theta \rangle$ as functions of time and of the peak intensity $I_{2\omega,0}$ of the 2ω-laser field computed by solving the time-dependent Schrödinger equation. The adiabatic results of the orientation and alignment are presented in (c) and (d), respectively. The peak intensity of the ω-laser field is $I_{\omega,0} = 3 \times 10^{11}$ W/cm^2.

expanded wave function is obtained by adding a phase shift to each eigenstate. More details of the method are described in Ref. [34].

To understand the field-dressed rotational dynamics, we have also performed AA calculations by solving the time-independent Schrödinger equation associated with the Hamiltonian for each time step. When the field intensity changes, since there are avoided crossings between energetically adjacent states with the same symmetry, the energy order of the eigenstates is preserved [32]. Hence we can clarify correspondences between the field-free states and their field-dressed states. The contribution of the adiabatic pendular eigenstates to the time-dependent wave function allows us to interpret the nonadiabatic dynamics.

III. FIELD-DRESSED ROTATIONAL DYNAMICS

In this section, we use the OCS molecule as a benchmark to illustrate our results, and we focus on its rotational ground state. The constants of OCS used in this work are $B = 0.203$ cm^{-1}, $\alpha_{zz} - \alpha_{xx} = 27.15$ a.u., $\beta_{zzz} = 45.0$ a.u., and $\beta_{zxx} = 59.1$ a.u. [37]. Note that we have used positive values for the hyperpolarizability components [37], so that the ground state becomes oriented i.e., $\langle \cos\theta \rangle > 0$. Here, the FWHM of the ω- and 2ω-laser pulses are fixed to 3 ns and 2 ns, respectively, and the peak intensity of the ω-laser field to $I_{\omega,0} = 3 \times 10^{11}$ W/cm^2.

A. Dynamics for two-color laser fields with parallel polarizations

We start by analyzing the rotational dynamics of the OCS ground state exposed to the two-color laser fields with parallel polarizations. The degrees of alignment and orientation along the Z axis are characterized by the expectation values $\langle \cos^2\theta \rangle$ and $\langle \cos\theta \rangle$, respectively. In Figs. 3(a) and 3(b), we present the time-dependent orientation and alignment as functions of the time and the peak intensity of the 2ω-laser field. The corresponding adiabatic results are shown in Figs. 3(c) and 3(d). The ground state shows a strong alignment at the peak of the two pulses. We confirm a good agreement between the time-dependent and adiabatic results as shown in Figs. 3(b) and 3(d).

There are significant differences between the time-dependent and adiabatic orientation as shown in Figs. 3(a) and 3(c), the former being smaller than the latter. These differences are a clear signature that the rotational dynamics is nonadiabatic [28,29]. To get better physical insight into the nonadiabatic orientation, we explore in detail the field-dressed rotational dynamics for a 2ω-laser pulse having the peak intensity of $I_{2\omega,0} = 5 \times 10^{11}$ W/cm^2, which is marked by dotted lines in the contour plots of Fig. 3. The orientation and alignment evolutions are plotted in Figs. 4(a) and 4(b). We observe that the TDSE and AA results of alignment show a very good agreement, in contrast to the results of the orientation.

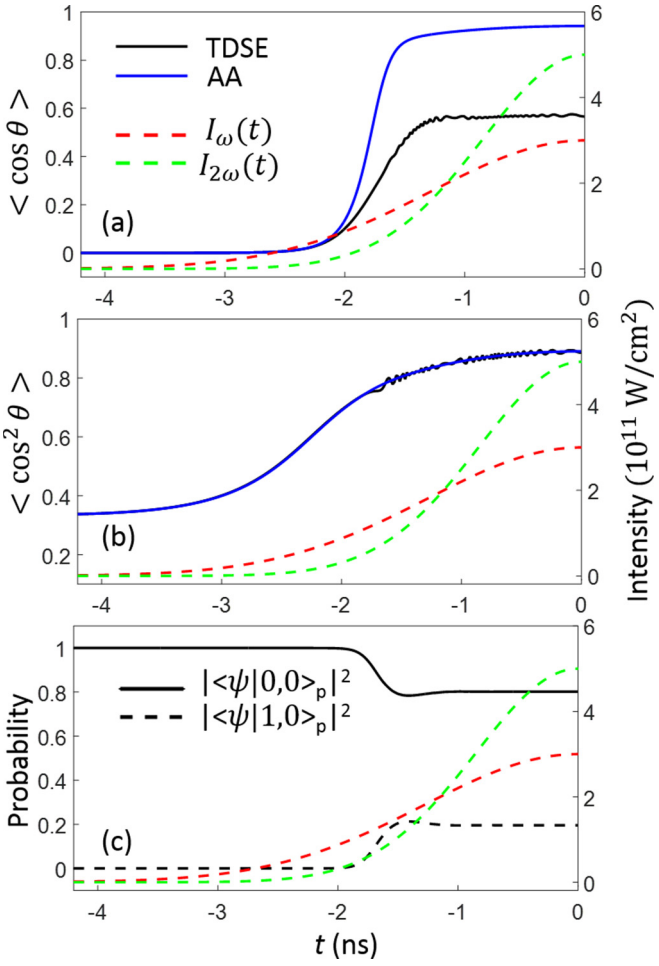

FIG. 4. For fixed peak intensities $I_{\omega,0} = 3 \times 10^{11}$ W/cm^2 and $I_{2\omega,0} = 5 \times 10^{11}$ W/cm^2, time evolutions of (a) orientation and (b) alignment, and (c) squares of the projections of the time-dependent wave function onto the adiabatic pendular states. The adiabatic results for the orientation and alignment, and temporal profiles of the two laser pulses are also plotted.

Due to the difference in the temporal widths, the molecules show a strong alignment $\langle\cos^2\theta\rangle \sim 0.7$ already at $t \approx -2.0$ ns, which is even before the interaction with the 2ω-laser field becomes significant. The rotational wave packet is equally confined to $\theta = 0$ and $\theta = \pi$ potential wells. In addition, a quasidegenerate pendular pair is formed between the field-dressed ground $|0,0\rangle_p$ and excited $|1,0\rangle_p$ states. In the two-color laser fields, these two states have the same symmetry and are coupled due to the interaction of the molecular hyperpolarizability with these fields. As time further goes by and the laser pulse intensities increase, the asymmetry of the interaction potential increases. As a consequence, a part of the rotational wave packet tunnels through the potential barrier from the shallow potential well ($\theta = \pi$) to the deeper one ($\theta = 0$), and the ground state gets oriented. The wave packet was initially formed only in the adiabatic pendular ground state $|0,0\rangle_p$. Due to its coupling with the energetically neighboring state $|1,0\rangle_p$, the populations are transferred between the two states, which now contribute to the change in the wave packet populations. Hence the field-dressed rotational dynamics is nonadiabatic.

This nonadiabatic dynamics is illustrated in Fig. 4(c), with the squares of the projections of the time-dependent wave function onto the two lowest-lying adiabatic pendular eigenstates of the full Hamiltonian at each time step. For $t \lesssim -2.0$ ns, the pendular ground state $|0,0\rangle_p$ has the dominant contribution to the wave packet, which is almost 1. Once the interaction with the 2ω-laser field becomes significant, a part of the population is transferred to the adiabatic pendular state $|1,0\rangle_p$, which is antioriented. This suppresses the net orientation, i.e., the value $\langle\cos\theta\rangle$, of the ground-state time-dependent wave function. For $t \gtrsim -1.3$ ns, the populations of the adiabatic states $|0,0\rangle_p$ and $|1,0\rangle_p$ remain constant at 0.804 and 0.196, respectively. In the adiabatic approximation, only the adiabatic ground state contributes to the field-dressed wave packet. Note that the two adiabatic states contributing to the time-dependent wave functions are oriented in opposite directions but have almost the same alignment. As a consequence, the nonadiabatic rotational dynamics is manifested only in the orientation but not in the alignment.

We emphasize that this nonadiabatic dynamics strongly depends on the FWHM, peak intensities, and temporal profiles of the laser fields. By comparing the results in panels (a) and (c) of Fig. 3, we observe that, for the considered range of the 2ω-laser field intensity, the AA calculations do not reproduce the TDSE orientation. This indicates that the rotational dynamics is nonadiabatic, which holds even for 2ω-laser intensities smaller than the ω-laser intensity of $I_{\omega,0} = 3 \times 10^{11}$ W/cm^2.

Analogous to the combined-field orientation [28,29,38,39], the adiabatic dynamics could be achieved by increasing the temporal widths of the two pulses significantly [28,40]. We note that, in Ref. [34], where the assumed laser pulses are four times longer than the ones used in the present work, the orientation dynamics can be quasiadiabatic by optimizing the intensities of the two wavelengths. The adiabaticity of orientation dynamics can be improved by optimizing the relative delay between the ω and 2ω laser pulses [34]. In the next subsection, another solution for achieving the quasiadiabatic and stronger orientation is provided.

B. Dynamics for two-color laser fields with perpendicular polarizations

For perpendicular fields, the orientation along the Z axis, and the alignment along the Z and X axes, i.e., $\langle\cos\theta\rangle$, $\langle\cos^2\theta\rangle$, and $\langle\sin^2\theta\cos^2\phi\rangle$, respectively, are presented in Fig. 5 as functions of the time and of the peak intensity of the 2ω-laser pulse. The peak intensity of the ω-laser field is $I_{\omega,0} = 3 \times 10^{11}$ W/cm^2. As in the parallel field configuration, we confirm a good agreement between the degrees of alignment computed by solving the TDSE, panels (b) and (c) of Fig. 5, and those computed by using the AA, panels (e) and (f) of Fig. 5. The corresponding field-dressed Hamiltonian $H = H_{\rm rot} + H_{\rm int}^{\perp}(t)$ does not have azimuthal symmetry, and the interaction with the two fields competes to align the molecules in mutually perpendicular directions. Indeed, the ground state is aligned along the Z or X axis if the interaction with the 2ω- or ω-laser field is dominant, respectively [compare the

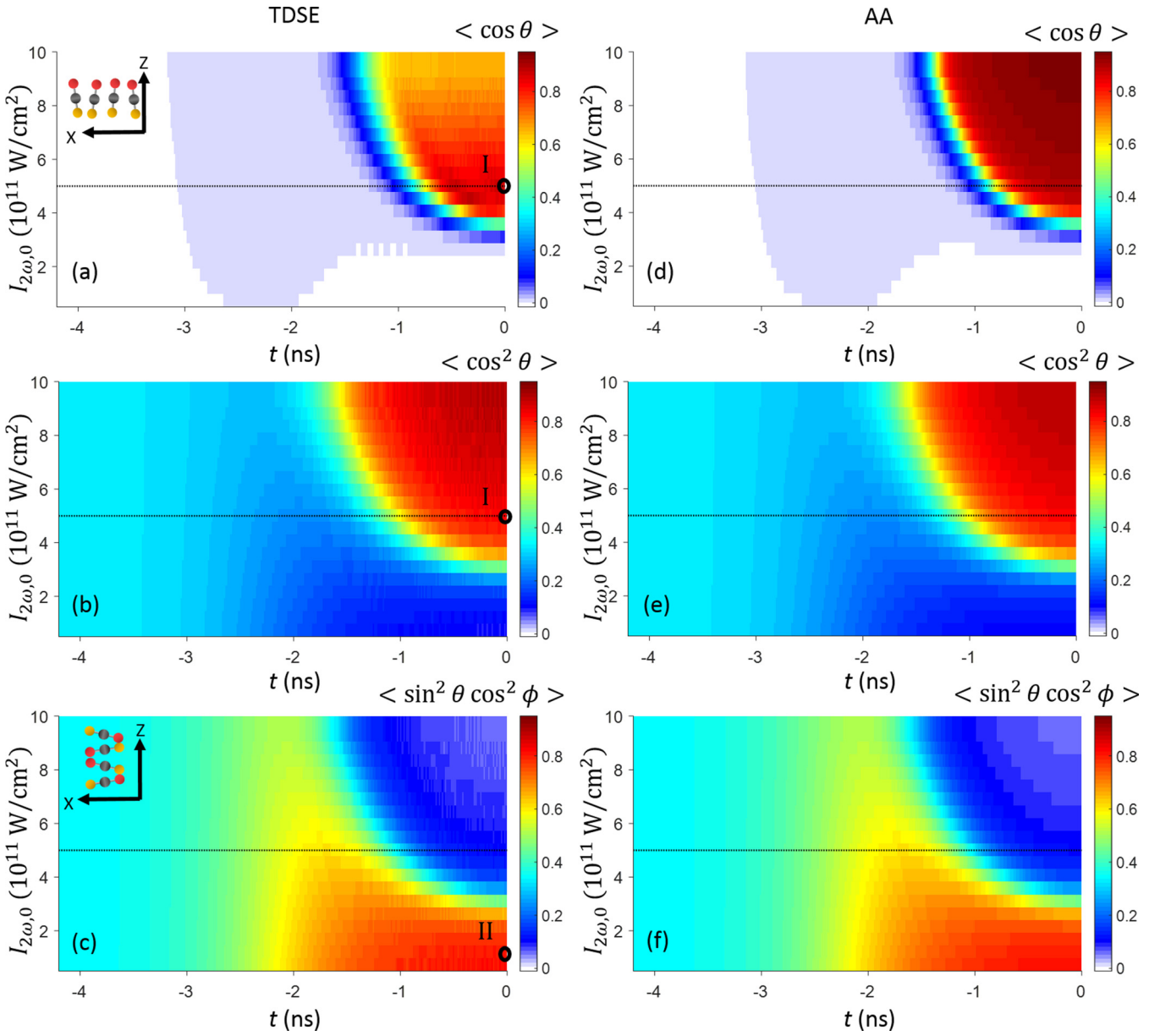

FIG. 5. For perpendicular fields, (a) orientation $\langle\cos\theta\rangle$, (b) alignment along the Z-axis $\langle\cos^2\theta\rangle$, and (c) alignment along the X-axis $\langle\sin^2\theta\,\cos^2\phi\rangle$ as functions of time and of the peak intensity $I_{2\omega,0}$ of the 2ω-laser field computed by solving the time-dependent Schrödinger equation. The adiabatic results of the orientation along the Z axis and the alignment along the Z and X axes are presented in (d), (e), and (f), respectively. The peak intensity of the ω-laser field is $I_{\omega,0} = 3 \times 10^{11}$ W/cm^2. In the perpendicular configuration, either orientation along the Z axis or alignment along the X axis can be created depending on time and the relative intensities of the ω- and 2ω-laser pulses. The inset in (a) illustrates that the molecules are oriented (and aligned) along the Z axis under the condition I marked in (a) and (b), where $t = 0$ ns and $I_{2\omega,0} = 5 \times 10^{11}$ W/cm^2, while the inset in (c) illustrates that the molecules are aligned along the X axis under the condition II marked in (c), where $t = 0$ ns and $I_{2\omega,0} = 1.5 \times 10^{11}$ W/cm^2.

insets in Figs. 5(a) and 5(c)]. We emphasize that molecules are not purely aligned along one direction. For $I_{\omega,0} = I_{2\omega,0}$, the molecules are almost equally aligned along the two axes, with $\langle\cos^2\theta\rangle = 0.459$ and $\langle\sin^2\theta\,\cos^2\phi\rangle = 0.456$ at the peak of the laser fields $t = 0$ ns; the ground state is then considered to be antialigned against the Y axis.

In contrast, the orientation is significant when the interaction with the 2ω-laser field is dominant, i.e., when the molecules are aligned along the Z axis [see the inset in Fig. 5(a)]. In addition, the AA calculation [see Fig. 5(d)] does not reproduce the time-dependent orientation presented in Fig. 5(a), which again indicates that the rotational dynamics is nonadiabatic. Compared to the parallel field configuration, stronger orientation is achieved. This stronger orientation can be explained in terms of a weaker alignment along the Z axis as a tradeoff, which is accompanied by a larger energy splitting in the lowest-lying pendular doublet, when the interaction with the 2ω-laser field starts to dominate. For

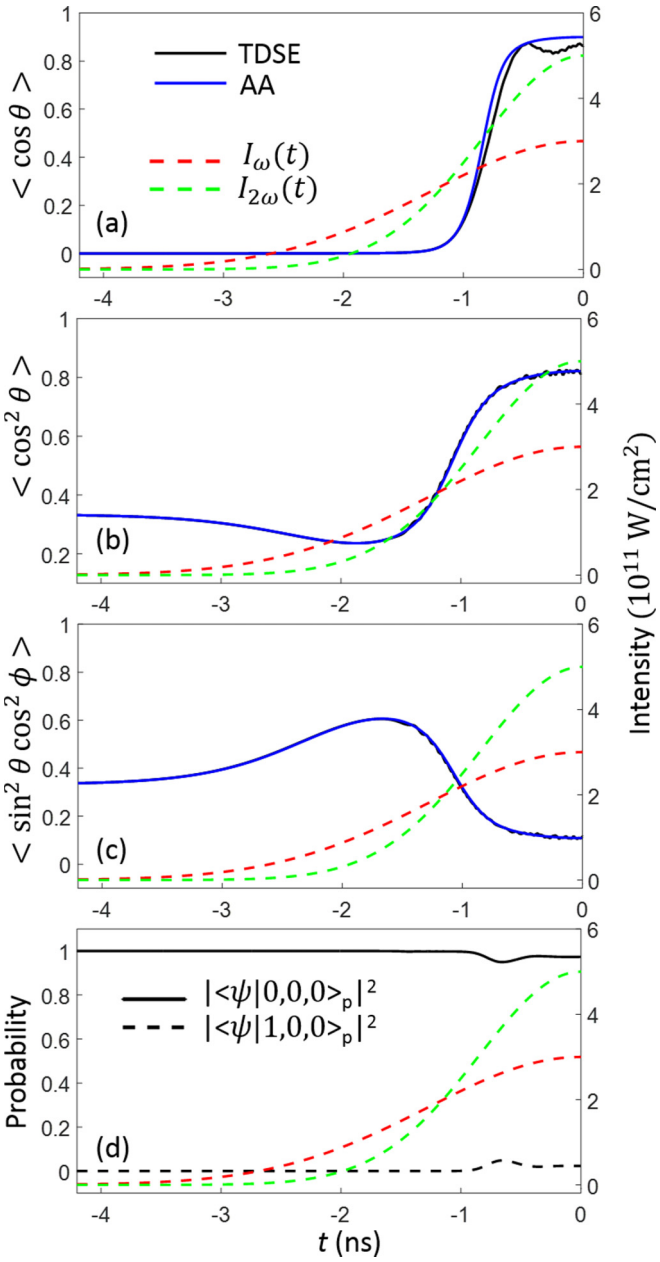

FIG. 6. For perpendicular fields and laser intensities $I_{\omega,0} = 3 \times 10^{11}$ W/cm^2 and $I_{2\omega,0} = 5 \times 10^{11}$ W/cm^2, time evolutions of (a) orientation, (b), (c) alignment along the Z and X axes, respectively, and (d) squares of the projections of the time-dependent wave function onto the adiabatic pendular states. The adiabatic results for the orientation and alignment and the temporal profiles of the two laser pulses are also plotted.

instance, $\langle\cos\theta\rangle = 0.566$ and $\langle\cos\theta\rangle = 0.862$ at $t = 0$ ns, for the parallel and perpendicular configurations, respectively, with $I_{\omega,0} = 3 \times 10^{11}$ W/cm^2 and $I_{2\omega,0} = 5 \times 10^{11}$ W/cm^2.

In Figs. 6(a)–6(d), we analyze in detail the nonadiabatic dynamics of the ground state for $I_{2\omega,0} = 5 \times 10^{11}$ W/cm^2 and $I_{\omega,0} = 3 \times 10^{11}$ W/cm^2. The corresponding dynamics are marked with dotted lines in the contour plots of Fig. 5. The alignment along the Z axis (X axis) initially decreases (increases) as time goes by, and reaches broad minimum (maximum) at $t \approx -1.68$ ns. As time further goes by, $\langle\cos^2\theta\rangle$ increases reaching a maximum at $t = 0$ ns, whereas $\langle\sin^2\theta\cos^2\phi\rangle$ reaches a minimum. These time evolutions of $\langle\cos^2\theta\rangle$ and $\langle\sin^2\theta\cos^2\phi\rangle$ illustrate the interplay between the interactions with the 2ω- and ω-laser fields as t passes. Indeed, at $t \approx -1.16$ ns, we find that $\langle\cos^2\theta\rangle \approx \langle\sin^2\theta\cos^2\phi\rangle \approx 0.445$. As t further goes by, the alignment along the Z axis increases because the interaction due to the 2ω-laser field becomes dominant.

The combination of the 2ω- and ω-laser fields forms a potential orienting the molecules in the $+Z$ direction. The orientation $\langle\cos\theta\rangle$ increases for $t \gtrsim -1$ ns, when the 2ω-laser field becomes stronger than the ω-laser field. We find a relatively good agreement between the time-dependent and adiabatic results. This can be explained in terms of the weaker alignment along the Z axis for $t \approx -1$ ns than that in the parallel-field configuration as shown in Fig. 4(b), which implies a large energy gap between the adiabatic states $|0, 0, 0\rangle_p$ and $|1, 0, 0\rangle_p$ forming the pendular pair. The large energy gap between the two states is associated with a better adiabatic criterion [28,29] for the corresponding rotational dynamics. From the perspective of the tunneling of the rotational wave packet between the two potential wells at $\theta = 0$ and $\theta = \pi$ [34], in the perpendicular-field configuration, the alignment and orientation along the Z axis are created at nearly the same time, giving rise to a quasiadiabatic rotational dynamics. Furthermore, the rotational wave packet has a larger probability to move due to the elaborate forms of the potential in the angular space as shown in Figs. 2(c) and 2(d), which have smaller potential wells.

In Fig. 6(d), we show the population distributions of the time-dependent wave function of the two adiabatic pendular states. Compared to the parallel-field configuration presented in Fig. 4(c), the population transferred from $|0, 0, 0\rangle_p$, which forms the wave packet when the dynamics is adiabatic, to $|1, 0, 0\rangle_p$ is much smaller. As in the parallel-field configuration, the difference between the time-dependent and adiabatic orientation dynamics becomes larger for higher intensities of $I_{2\omega,0}$ as shown in Figs. 5(a) and 5(d), which illustrates that the nonadiabatic dynamics strongly depends on the field parameters.

IV. SUMMARY AND OUTLOOK

In this work, we have investigated the rotational dynamics of OCS molecules in the presence of two-color laser fields with the parallel and perpendicular polarizations. In particular, we have analyzed the degrees of orientation and alignment of the ground state as functions of the peak intensity of the 2ω-laser field and of time. Together with the time-dependent analysis of the field-dressed rotational dynamics, we also present an adiabatic rotational dynamics.

For the parallel-field configuration, the ground state shows a significant alignment at $t = 0$, but a moderate orientation. A comparison between the time-dependent and adiabatic analyses has proved that the field-dressed rotational dynamics is not adiabatic. We have shown that a nonadiabatic transfer of the population takes place when the interaction with the 2ω-laser field becomes significant, and the laser intensities further increase. Compared to a fully adiabatic rotational dynamics,

the degree of orientation obtained by solving the TDSE is significantly suppressed. This is explained in terms of the transfer of population from the ground pendular state to the first excited pendular state, which is antioriented.

For perpendicular fields, the ground state is aligned along the X or Z axis if the interaction with the ω- or 2ω-laser field is dominant, respectively. Due to this interplay between the interactions with the two fields, the orientation reached at $t = 0$ is stronger than in the parallel-field configuration. Most important, we have found a range of field parameters, which are more favorable for realizing an adiabatic field-dressed dynamics. The method proposed here for achieving quasiadiabatic control of the orientation dynamics of the ground-state molecules is generally applicable to a thermal molecular ensemble [34].

The field-dressed rotational dynamics has been discussed so far in the literature for two-color lasers having parallel polarizations. In this work, we have shown that many unexplored opportunities to control the molecular dynamics emerge by using perpendicular fields or even more elaborate field configurations. Actually, the advantage of the combination of a linearly polarized ω-laser field and an elliptically polarized 2ω-laser field has been discussed in Ref. [41]. Three-dimensional orientation of asymmetric top molecules, which was demonstrated by the technique with combined electrostatic and elliptically polarized laser fields [21,33,42–44], has recently been achieved by the all-optical technique with the crossed-polarization configuration [45]. In addition, postpulse dynamics induced after two-color laser pulses having short temporal widths or with a rapid turn off [46–48] could be significantly affected by changing the polarization direction of one or both of the two-color laser pulses. Recently, it has been reported that two one-color pulses with perpendicular polarizations can be used for orienting angular momentum of linear molecules, i.e., unidirectional rotation of linear molecules [49–51]. Furthermore, if a molecule has off-diagonal components of the polarizability tensor, one-color laser pulses with crossed or orthogonal polarizations can be used not only for the orientation of the molecular angular momentum but also for the orientation of the molecules themselves [52,53]. Therefore, our two-color field approach with perpendicularly crossed polarizations can generalize the controlling techniques of unidirectional molecular rotation to the oriented molecules.

ACKNOWLEDGMENTS

J.H.M. is grateful to Professor Jochen Küpper, Dr. Yuanpin Chang, and Dr. Juan José Omiste for their help in developing a simulation code used in the present work. He was supported by the Institute for Basic Science under IBS-R012-D1. This study has been partially financed by the Consejería de Conocimiento, Investigación y Universidad, Junta de Andalucía and European Regional Development Fund (ERDF), ref. SOMM17/6105/UGR. R.G.F. gratefully acknowledges financial support by the Spanish Project No. FIS2017-89349-P (MINECO), and by the Andalusian research group FQM-207.

APPENDIX A: MOLECULAR AND LABORATORY FIXED FRAMES

The transformation between the laboratory-fixed frame (X, Y, Z) and the molecule-fixed frame (x, y, z) is given by [54]

$$\begin{pmatrix} x \\ y \\ z \end{pmatrix} = \begin{pmatrix} \mathrm{c}\phi\mathrm{c}\theta\mathrm{c}\chi - \mathrm{s}\phi\mathrm{s}\chi & \mathrm{s}\phi\mathrm{c}\theta\mathrm{c}\chi + \mathrm{c}\phi\mathrm{s}\chi & -\mathrm{s}\theta\mathrm{c}\chi \\ -\mathrm{c}\phi\mathrm{c}\theta\mathrm{s}\chi - \mathrm{s}\phi\mathrm{c}\chi & -\mathrm{s}\phi\mathrm{c}\theta\mathrm{s}\chi + \mathrm{c}\phi\mathrm{c}\chi & \mathrm{s}\theta\mathrm{s}\chi \\ \mathrm{c}\phi\mathrm{s}\theta & \mathrm{s}\phi\mathrm{s}\theta & \mathrm{c}\theta \end{pmatrix} \begin{pmatrix} X \\ Y \\ Z \end{pmatrix}, \tag{A1}$$

where θ is the polar angle between the molecular axis, i.e., the z axis of the molecule-fixed frame, and the Z axis in the laboratory-fixed frame. ϕ is defined as the angle between the X axis and the projection of the z axis to the XY plane and χ represents the rotated angle of the molecule with respect to the z axis. c and s stand for cosine and sine functions, respectively. Linear molecules are symmetric with respect to the rotation around the molecule-fixed z axis and χ can be given as a constant, which is fixed at zero in this work.

APPENDIX B: MATRIX ELEMENTS OF THE HAMILTONIAN

In this Appendix, we provide the matrix elements of different terms appearing in the field-free and interaction Hamiltonians H_{rot} and H_{int}.

The rigid-rotor Hamiltonian has a nonzero diagonal element given by

$$\langle J, M|\vec{J}^{\,2}|J, M\rangle = J(J+1).$$

For the matrix elements of the interaction Hamiltonian, $\langle J', M'|H_{\mathrm{int}}|J, M\rangle$, we use the integral of three spherical harmonics [54]

$$\int d\Omega Y_{J_3,M_3}(\theta,\phi) Y_{J_2,M_2}(\theta,\phi) Y_{J_1,M_1}(\theta,\phi) = \left[\frac{(2J_1+1)(2J_2+1)(2J_3+1)}{4\pi}\right]^{\frac{1}{2}} \begin{pmatrix} J_1 & J_2 & J_3 \\ 0 & 0 & 0 \end{pmatrix} \begin{pmatrix} J_1 & J_2 & J_3 \\ M_1 & M_2 & M_3 \end{pmatrix},$$

where $\left(\begin{smallmatrix} a & b & c \\ d & e & f \end{smallmatrix}\right)$ are Wigner-3j symbols.

The functions $\cos\theta$, $\cos^2\theta$, and $\sin^2\theta\cos 2\phi$ are expressed in terms of the spherical harmonics $Y_{1,0}(\theta,\phi)$, $Y_{2,0}(\theta,\phi)$, and $Y_{2,\pm2}(\theta,\phi)$, respectively, whereas the functions $\cos^3\theta$ and $\sin^2\theta\cos\theta\cos 2\phi$ are expressed as the combinations of $Y_{3,0}(\theta,\phi)$ and $Y_{1,0}(\theta,\phi)$, and of $Y_{3,+2}(\theta,\phi)$ and $Y_{3,-2}(\theta,\phi)$, respectively.

The resultant nonzero matrix elements are

$$\langle J,M|\cos\theta|J+1,M\rangle = \sqrt{\frac{(J+1+M)(J+1-M)}{(2J+1)(2J+3)}},$$

$$\langle J,M|\cos^2\theta|J,M\rangle = \frac{1}{3}+\frac{2[J(J+1)-3M^2]}{3(2J+3)(2J-1)},$$

$$\langle J,M|\cos^2\theta|J+2,M\rangle = \sqrt{\frac{[(J+1)^2-M^2][(J+2)^2-M^2]}{(2J+1)(2J+3)^2(2J+5)}},$$

$$\langle J,M|\sin^2\theta\ \cos 2\phi|J+2,M+2\rangle = \frac{1}{2}\sqrt{\frac{(J+1+M)(J+2+M)(J+3+M)(J+4+M)}{(2J+1)(2J+3)^2(2J+5)}},$$

$$\langle J,M|\sin^2\theta\ \cos 2\phi|J+2,M-2\rangle = \frac{1}{2}\sqrt{\frac{(J+1-M)(J+2-M)(J+3-M)(J+4-M)}{(2J+1)(2J+3)^2(2J+5)}},$$

$$\langle J,M|\sin^2\theta\ \cos 2\phi|J,M+2\rangle = -\frac{\sqrt{(J+M+1)(J+M+2)(J-M-1)(J-M)}}{(2J-1)(2J+3)},$$

$$\langle J,M|\cos^3\theta|J+3,M\rangle = \sqrt{\frac{(J+3+M)(J+3-M)}{(2J+5)(2J+7)}}\langle J,M|\cos^2\theta|J+2,M\rangle,$$

$$\langle J,M|\cos^3\theta|J+1,M\rangle = \sqrt{\frac{(J+2+M)(J+2-M)}{(2J+3)(2J+5)}}\langle J,M|\cos^2\theta|J+2,M\rangle + \sqrt{\frac{(J+1+M)(J+1-M)}{(2J+1)(2J+3)}}\langle J,M|\cos^2\theta|J,M\rangle,$$

$$\langle J,M|\sin^2\theta\cos\theta\ \cos 2\phi|J+3,M+2\rangle = \sqrt{\frac{(J+M+5)(J-M+1)}{(2J+5)(2J+7)}}\langle J,M|\sin^2\theta\ \cos 2\phi|J+2,M+2\rangle,$$

$$\langle J,M|\sin^2\theta\cos\theta\ \cos 2\phi|J+3,M-2\rangle = \sqrt{\frac{(J+M+1)(J-M+5)}{(2J+5)(2J+7)}}\langle J,M|\sin^2\theta\ \cos 2\phi|J+2,M-2\rangle,$$

$$\begin{aligned}\langle J,M|\sin^2\theta\cos\theta\ \cos 2\phi|J+1,M+2\rangle &= \sqrt{\frac{(J+M+4)(J-M)}{(2J+3)(2J+5)}}\langle J,M|\sin^2\theta\ \cos 2\phi|J+2,M+2\rangle \\ &+\sqrt{\frac{(J+M+3)(J-M-1)}{(2J+1)(2J+3)}}\langle J,M|\sin^2\theta\ \cos 2\phi|J,M+2\rangle,\end{aligned}$$

$$\begin{aligned}\langle J,M|\sin^2\theta\cos\theta\ \cos 2\phi|J+1,M-2\rangle &= \sqrt{\frac{(J+M)(J-M+4)}{(2J+3)(2J+5)}}\langle J,M|\sin^2\theta\ \cos 2\phi|J+2,M-2\rangle \\ &+\sqrt{\frac{(J+M-1)(J-M+3)}{(2J+1)(2J+3)}}\langle J,M|\sin^2\theta\ \cos 2\phi|J,M-2\rangle.\end{aligned}$$

The other matrix elements used in this work can be evaluated by combining the above matrix elements.

[1] T. Suzuki, S. Minemoto, T. Kanai, and H. Sakai, Phys. Rev. Lett. **92**, 133005 (2004).

[2] L. Holmegaard, J. L. Hansen, L. Kalhøj, S. Louise Kragh, H. Stapelfeldt, F. Filsinger, J. Küpper, G. Meijer, D. Dimitrovski,

M. Abu-samha, C. P. J. Martiny, and L. Bojer Madsen, Nat. Phys. **6**, 428 (2010).
[3] J. Itatani, J. Levesque, D. Zeidler, H. Niikura, H. Pépin, J. C. Kieffer, P. B. Corkum, and D. M. Villeneuve, Nature (London) **432**, 867 (2004).
[4] T. Kanai, S. Minemoto, and H. Sakai, Nature (London) **435**, 470 (2005).
[5] T. Kanai, S. Minemoto, and H. Sakai, Phys. Rev. Lett. **98**, 053002 (2007).
[6] C. Vozzi, M. Negro, F. Calegari, G. Sansone, M. Nisoli, S. De Silvestri, and S. Stagira, Nat. Phys. **7**, 822 (2011).
[7] B. Friedrich and D. Herschbach, Phys. Rev. Lett. **74**, 4623 (1995).
[8] B. Friedrich and D. Herschbach, J. Phys. Chem. **99**, 15686 (1995).
[9] B. Friedrich and D. Herschbach, J. Chem. Phys. **111**, 6157 (1999).
[10] B. Friedrich and Herschbach, J. Phys. Chem. A **103**, 10280 (1999).
[11] H. Sakai, S. Minemoto, H. Nanjo, H. Tanji, and T. Suzuki, Phys. Rev. Lett. **90**, 083001 (2003).
[12] S. Minemoto, H. Nanjo, H. Tanji, T. Suzuki, and H. Sakai, J. Chem. Phys. **118**, 4052 (2003).
[13] L. Holmegaard, J. H. Nielsen, I. Nevo, H. Stapelfeldt, F. Filsinger, J. Küpper, and G. Meijer, Phys. Rev. Lett. **102**, 023001 (2009).
[14] T. Kanai and H. Sakai, J. Chem. Phys. **115**, 5492 (2001).
[15] K. Oda, M. Hita, S. Minemoto, and H. Sakai, Phys. Rev. Lett. **104**, 213901 (2010).
[16] C.-C. Shu, K.-J. Yuan, W.-H. Hu, and S.-L. Cong, J. Chem. Phys. **132**, 244311 (2010).
[17] S. Fleischer, Y. Zhou, R. W. Field, and K. A. Nelson, Phys. Rev. Lett. **107**, 163603 (2011).
[18] K. Kitano, N. Ishii, and J. Itatani, Phys. Rev. A **84**, 053408 (2011).
[19] F. Filsinger, J. Küpper, G. Meijer, L. Holmegaard, J. H. Nielsen, I. Nevo, J. L. Hansen, and H. Stapelfeldt, J. Chem. Phys. **131**, 064309 (2009).
[20] J. H. Mun, D. Takei, S. Minemoto, and H. Sakai, Phys. Rev. A **89**, 051402(R) (2014).
[21] D. Takei, J. H. Mun, S. Minemoto, and H. Sakai, Phys. Rev. A **94**, 013401 (2016).
[22] O. Ghafur, A. Rouzée, A. Gijsbertsen, W. K. Siu, S. Stolte, and M. J. J. Vrakking, Nat. Phys. **5**, 289 (2009).
[23] J. Wu and H. Zeng, Phys. Rev. A **81**, 053401 (2010).
[24] S. Zhang, C. Lu, T. Jia, Z. Wang, and Z. Sun, Phys. Rev. A **83**, 043410 (2011).
[25] P. M. Kraus, A. Rupenyan, and H. J. Wörner, Phys. Rev. Lett. **109**, 233903 (2012).
[26] P. M. Kraus, D. Baykusheva, and H. J. Wörner, J. Phys. B: At., Mol., Opt. Phys. **47**, 124030 (2014).
[27] K. Sonoda, A. Iwasaki, K. Yamanouchi, and H. Hasegawa, Chem. Phys. Lett. **693**, 114 (2018).
[28] J. H. Nielsen, H. Stapelfeldt, J. Küpper, B. Friedrich, J. J. Omiste, and R. González-Férez, Phys. Rev. Lett. **108**, 193001 (2012).
[29] J. J. Omiste and R. González-Férez, Phys. Rev. A **86**, 043437 (2012).
[30] J. J. Omiste, M. Gärttner, P. Schmelcher, R. González-Férez, L. Holmegaard, J. H. Nielsen, H. Stapelfeldt, and J. Küpper, Phys. Chem. Chem. Phys. **13**, 18815 (2011).
[31] J. J. Omiste and R. González-Férez, Phys. Rev. A **88**, 033416 (2013).
[32] J. J. Omiste, R. González-Férez, and P. Schmelcher, J. Chem. Phys. **135**, 064310 (2011).
[33] J. L. Hansen, J. J. Omiste, J. H. Nielsen, D. Pentlehner, J. Küpper, R. González-Férez, and H. Stapelfeldt, J. Chem. Phys. **139**, 234313 (2013).
[34] J. H. Mun and H. Sakai, Phys. Rev. A **98**, 013404 (2018).
[35] N. Takemoto and K. Yamanouchi, Chem. Phys. Lett. **451**, 1 (2008).
[36] A. D. Buckingham, *Advances in Chemical Physics* (John Wiley & Sons, New York, 2007), pp. 107–142.
[37] G. Maroulis and M. Menadakis, Chem. Phys. Lett. **494**, 144 (2010).
[38] Y. Sugawara, A. Goban, S. Minemoto, and H. Sakai, Phys. Rev. A **77**, 031403(R) (2008).
[39] J. S. Kienitz, S. Trippel, T. Mullins, K. Dlugolecki, R. González-Férez, and J. Küpper, ChemPhysChem **17**, 3740 (2016).
[40] M. Muramatsu, M. Hita, S. Minemoto, and H. Sakai, Phys. Rev. A **79**, 011403(R) (2009).
[41] M. M. Hossain, Ph.D. thesis, The University of Tokyo, 2019.
[42] H. Tanji, S. Minemoto, and H. Sakai, Phys. Rev. A **72**, 063401 (2005).
[43] A. S. Chatterley, B. Shepperson, and H. Stapelfeldt, Phys. Rev. Lett. **119**, 073202 (2017).
[44] L. V. Thesing, J. Küpper, and R. González-Férez, J. Chem. Phys. **146**, 244304 (2017).
[45] K. Lin, I. Tutunnikov, J. Qiang, J. Ma, Q. Song, Q. Ji, W. Zhang, H. Li, F. Sun, X. Gong, H. Li, P. Lu, H. Zeng, Y. Prior, I. Sh. Averbukh, and J. Wu, Nat. Commun. **9**, 5134 (2018).
[46] A. Goban, S. Minemoto, and H. Sakai, Phys. Rev. Lett. **101**, 013001 (2008).
[47] J. G. Underwood, M. Spanner, M. Y. Ivanov, J. Mottershead, B. J. Sussman, and A. Stolow, Phys. Rev. Lett. **90**, 223001 (2003).
[48] A. S. Chatterley, E. T. Karamatskos, C. Schouder, L. Christiansen, A. V. Jørgensen, T. Mullins, J. Küpper, and H. Stapelfeldt, J. Chem. Phys. **148**, 221105 (2018).
[49] S. Fleischer, Y. Khodorkovsky, Y. Prior, and I. S. Averbukh, New J. Phys. **11**, 105039 (2009).
[50] K. Kitano, H. Hasegawa, and Y. Ohshima, Phys. Rev. Lett. **103**, 223002 (2009).
[51] G. Karras, M. Ndong, E. Hertz, D. Sugny, F. Billard, B. Lavorel, and O. Faucher, Phys. Rev. Lett. **114**, 103001 (2015).
[52] E. Gershnabel and I. Sh. Averbukh, Phys. Rev. Lett. **120**, 083204 (2018).
[53] I. Tutunnikov, E. Gershnabel, S. Gold, and I. Sh. Averbukh, J. Phys. Chem. Lett. **9**, 1105 (2018).
[54] R. N. Zare, *Angular Momentum: Understanding Spatial Aspects in Chemistry and Physics* (John Wiley & Sons, New York, 1988), pp. 79–81.